J|A|C|S COMMUNICATIONS

Published on Web 05/14/2010

The Transition between Conformal Atomic Layer Epitaxy and Nanowire Growth

Ren Bin Yang,*,† Nikolai Zakharov,† Oussama Moutanabbir,† Kurt Scheerschmidt,† Li-Ming Wu,§ Ulrich Gösele,†,|| Julien Bachmann,*,†,‡ and Kornelius Nielsch‡

Max Planck Institute of Microstructure Physics, Weinberg 2, 06120 Halle, Germany, Institute of Applied Physics, University of Hamburg, Jungiusstr. 11, 20355 Hamburg, Germany, and State Key Laboratory of Structural Chemistry, Fujian Institute of Research on the Structure of Matter, Chinese Academy of Sciences, Fuzhou, Fujian 350002, P. R. China

Received March 28, 2010; E-mail: renbin@gmail.com; julien.bachmann@physik.uni-hamburg.de

Atomic layer deposition (ALD) is a thin-film technique based on complementary surface reactions between two thermally stable but mutually reactive gaseous molecules introduced in alternating fashion into the reaction chamber.[1] It offers the unique possibility of coating substrates of complex geometries *conformally*. The vapor−liquid−solid mechanism (VLS), on the other hand, occurs when gas molecules thermally decompose into their elements at a catalytic droplet and dissolve into it to form a eutectic mixture from which the desired solid crystallizes.[2] Here, the growth is *anisotropic* and yields nanowires. Although conformal and anisotropic modes of deposition are opposed in most aspects, we demonstrate in this work the possibility of a continuous transition between them, and we apply the insight gleaned from our investigation to the creation of original wire heterostructures.

Nanowire junctions, the functional building blocks for creating devices,[3] are created most simply in either the axial or radial direction (two segments or core−shell). The former structure is usually grown in VLS mode at a temperature slightly above the relevant eutectic temperature but usually below the temperature for uncatalyzed decomposition of the precursor molecules. In contrast to this, a shell is usually grown around an existing wire at an elevated temperature in order to allow for efficient, uncatalyzed, isotropic decomposition of the precursors. The effect of the catalyst particle may in that case result in a tapered nanowire.[4] The self-limiting nature of ALD, the alternative for growing a shell, necessitates that uniform coatings, mostly amorphous ones, be obtained. Crystalline coatings have been obtained under the label "atomic layer epitaxy" (ALE) at growth temperatures typically ≥300 °C.[5]

The testbed chosen for our study was a material system of relevance to thermoelectric and photovoltaic applications: antimony sulfide/selenide.[6] For Sb_2S_3, we were able to establish both the ALD and VLS growth modes from a single set of precursors, namely, tris(dimethylamino)antimony, $(Me_2N)_3Sb$, and hydrogen sulfide, H_2S, at 90 and 350 °C, respectively.[7] This implies that between those two temperatures, the system undergoes a transition from ALD to VLS. We first used as the substrate Sb_2Se_3 nanowires grown by 500 cycles of Au-catalyzed pulsed VLS (Figure 1a). These nanowires were single-crystalline with the *c* axis of the orthorhombic structure parallel to their long axis. After the nanowires were cooled, 500 cycles of Sb_2S_3 ALD carried out at 90 °C deposited a homogeneous shell, as is evident from the increased diameter shown in the scanning electron microscopy (SEM) image in Figure 1b. The transmission electron microscopy (TEM) image in Figure 1c shows that the entire nanowire structure, including the gold catalyst, was covered with a smooth shell having a thickness of 25−30 nm, consistent with isotropic ALD growth at the

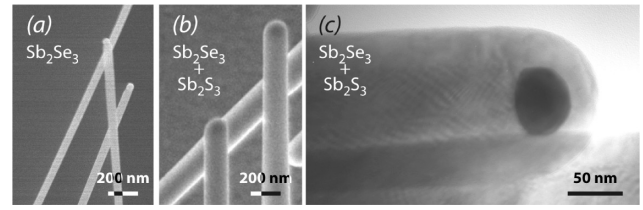

Figure 1. Conformal heteroepitaxial deposition of Sb_2S_3 at 90 °C onto Sb_2Se_3 wires. (a, b) SEM and (c) TEM images of (a) the substrate and (b, c) the core−shell wires.

previously determined deposition rate (0.58 Å cycle^{-1}).[7a] The energy-dispersive X-ray fluorescence (EDX) line scan performed perpendicular to the longitudinal direction revealed a sharp interface between the Sb_2Se_3 core and the Sb_2S_3 shell (Figure 2a). No Se was detected in the shell. The atomic planes visible in the shell by high-resolution TEM (HRTEM; Figure 2b) reveal that in contrast to our ALD of Sb_2S_3 performed between 65 and 150 °C on other substrates, the ALD layer on the Sb_2Se_3 wires was crystalline and consisted of one solid crystal with its *c* direction running parallel to the long axis, including on the Au sphere. This establishes the *low-temperature ALE* of Sb_2S_3 on a nonplanar single-crystalline substrate. The epitaxy is made possible by the common crystal structure of Sb_2S_3 and Sb_2Se_3. The almost isotropic lattice mismatch of 3−4%, however, must cause a very significant elastic strain. The crystallinity of both the selenide and sulfide components in the core−shell structures was confirmed on the ensemble scale spectroscopically (Figure S1 in the Supporting Information). In micro-Raman spectroscopy, the core−shell sample featured

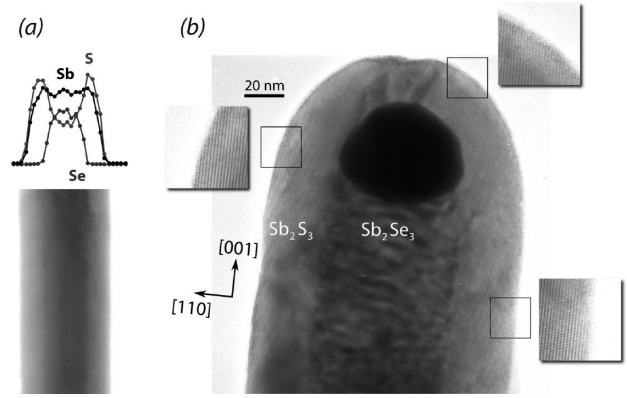

Figure 2. Conformal heteroepitaxial deposition of Sb_2S_3 at 90 °C onto Sb_2Se_3 wires. (a) EDX line scan across a core−shell wire (pictured underneath the graph); the vertical axis displays the signal intensities recorded for the elements Se, Sb, and S in purple, black, and green, respectively. (b) HRTEM image of the extremity of a wire, displaying the dark Au particle and identifying the crystallographic *c* axis parallel to the long axis of the wire.

† Max Planck Institute of Microstructure Physics.
§ Fujian Institute of Research on the Structure of Matter.
‡ University of Hamburg.
|| Deceased Nov 8, 2009.

10.1021/ja102590v

signals observed from the pure wires (186 and 252 cm^{-1} for Sb_2Se_3; 147, 278, and 302 cm^{-1} for Sb_2S_3) without the broadening that would be expected from the presence of amorphous or intermixed material.[8]

A change in the growth morphology was observed at the slightly more elevated temperature of 120 °C. The sample obtained after the Sb_2Se_3 wires were subjected to the conditions of Sb_2S_3 ALD at 120 °C (500 cycles; Figure 3) showed a shell radially encapsulating the selenide wires but also a considerable axial overgrowth at the tip. This axial elongation occurred at the expense of the Sb_2Se_3/Au interface: the metal catalyst was pushed sideways. Finally, when the experiment was repeated at 160 °C, the growth of Sb_2Se_3 became purely uniaxial in the crystallographic *c* direction. When 500 growth cycles were carried out at 160 °C, a new segment with a length of several hundred nanometers and a diameter similar to that of the selenide segment elongated the wire from its tip (Figure 4). The Au particle remained on the side at the height of the interface. EDX line scans attested to the complete absence of radial growth within the last micrometer of the structures, the purity of each segment, and the sharpness of the interface perpendicular to the long axis of the structure. Inspection of the wires at larger distances from the tips, however, revealed the presence of Sb_2S_3 remnants randomly distributed as small crystallites on the sides. In HRTEM images, no grain boundary was observed at the selenide−sulfide interface, although a small number of wires displayed a crack at the interface (Figure S2), most likely originating from the epitaxial strain caused by the lattice mismatch between sulfide and selenide.

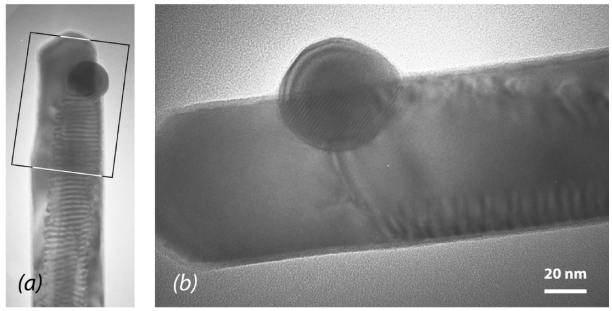

Figure 3. At 120 °C, conformal and anisotropic heteroepitaxial growths of Sb_2S_3 onto Sb_2Se_3 wires coexist, as shown by (a) TEM and (b) HRTEM images of one such structure. The region of (a) chosen for closer investigation in (b) is marked by a rectangle.

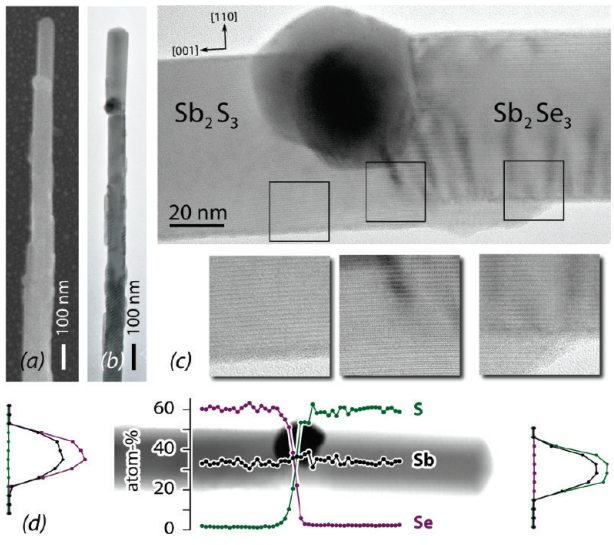

Figure 4. Perfectly anisotropic heteroepitaxial deposition of Sb_2S_3 onto Sb_2Se_3 wires at 160 °C. (a) SEM and (b) TEM images. (c) HRTEM images near the interface, in which no crystal defect is visible. (d) EDX linescans of the segmented wire. The radial scans show the absence of S (green) in the Sb_2Se_3 segment and of Se (purple) in Sb_2S_3; the axial scan, scaled to display the stoichiometry, shows an interface more abrupt than the EDX resolution.

A clarification is needed before a model is put forth to account for these observations. Indeed, the low decomposition temperatures of some amorphous V−VI compounds, whereby loss of the group VI element takes place, suggests that Se might be exchanged for S under the conditions of Sb_2S_3 ALD. However, this scenario can be excluded on the basis of experiments in which Sb_2Se_3 wires were kept at 160 °C overnight either under continuous pumping or with hydrogen sulfide regularly pulsed into the vacuum. Both procedures left the wires and the gold tips unscathed structurally and without trace of S in EDX line scans. Thus, we conclude that the Sb_2S_3 material obtained after the $(Me_2N)_3Sb + H_2S$ step (whether at 90, 120, or 160 °C) was exclusively deposited onto the selenide substrate. The crystallinity of the sulfide deposit observed at 90 °C contrasts with the results obtained in the case of amorphous substrates and suggests that the deposited solid has a significant mobility and crystallizes quickly during the deposition. Increasing the temperature thus enhances surface diffusion during deposition and thereby emphasizes the consequences of the lattice driving force over those of the chemical reaction. The larger thermal budget enables the crystal facet of highest energy to attract material from the other faces. We found by density functional theory methods that the surface tensions of both Sb_2S_3 and Sb_2Se_3 are larger on their *c* planes (at the wire extremities) than on the *a* and *b* planes (on the sides of the cylinder) by 20−58%,[9] in agreement with the experimental results available.[10] At the higher temperature, the crystal directs the growth, which becomes completely anisotropic: the tip collects the material initially deposited along the whole wire, as may also be the case in some cases of standard VLS growth.[11] We note the possible advantages offered by this method of growing segmented wires in comparison with the traditional consecutive VLS steps. First, it directly prevents the undesired incorporation of catalyst material into the second segment and its concomitant tapering.[12] Second, all of the material dissolved in the catalyst drop crystallizes out of it upon cooling before the second growth step. This elegantly circumvents the "reservoir" effect that otherwise smears out the interface.[13] The mechanism driving the lateral motion of the catalyst cannot be determined from our data. Such motion has, however, been investigated previously in other materials systems.[14] It was shown to arise when gold has a lower interfacial energy with the first segment than with the second one.

If the considerations above are correct and also apply to the homoepitaxy of Sb_2S_3, then we can foresee the appearance of a novel geometry. Indeed, VLS-grown Sb_2S_3 wires furnish a substrate complementary to their Sb_2Se_3 counterparts in that they mostly grow in the *b* direction (instead of *c*), as shown by HRTEM (Figure S3). Thus, homoepitaxial *c*-selective deposition at 160 °C should result in *anisotropic lateral growth*. Indeed, after deposition at 160 °C onto the *c* faces exposed on the sides, the wire cross section is a rectangle. Its shorter side equals the diameter of the gold catalyst, which is left at the tip (Figure 5c−e). The temperature for the onset of anisotropic growth (65−90 °C) is lower than in the heteroepitaxial case. This difference may originate from the diffusion distances, which are micrometers along the length of a wire but only tens of nanometers on its sides.

Thus, our observations indicate that on a suitable substrate, the crystal energy becomes prevalent in the thermodynamics of the thin-film growth initially thought of as "atomic layer deposition". Surface diffusion enables the experimentalist to balance it with the ubiquitous driving force of the chemical reaction to obtain epitaxial growth at exceptionally low temperatures. Furthermore, one can take control of the growth morphology and tune it at will between completely

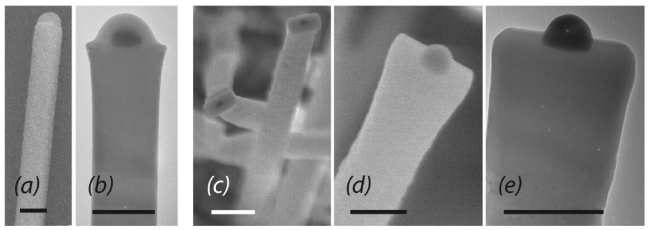

Figure 5. Homoepitaxial deposition of Sb_2S_3 is isotropic at 65 °C (a, b) and results in a cylindrical structure, whereas at 160 °C (c−e) it is selective for the *c* plane and yields wires with a rectangular cross section. Scale bars: 200 nm. (a, c, d) SEM images; (b, e) TEM images.

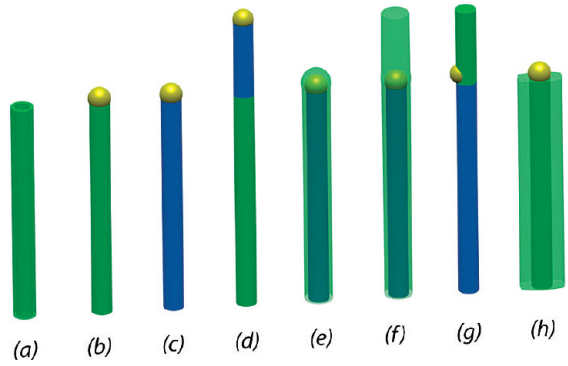

Figure 6. Structural variety of elongated antimony sulfide and selenide achieved under various growth conditions and combinations: (a) tubes by ALD in a porous template;[7b] (b, c) Sb_2S_3 and Sb_2Se_3 wires by VLS;[7a] (d) segmented wires by two consecutive VLS steps;[7a] (e) core−shell wire by conformal heteroepitaxy of Sb_2S_3 on Sb_2Se_3 at 90 °C (Figures 1 and 2); (f) segmented wire with core−shell component by deposition of Sb_2Se_3 at 120 °C (Figure 3); (g) segmented wires by anisotropic heteroepitaxy of Sb_2S_3 on Sb_2Se_3 at 160 °C (Figure 4); (h) rectangular wires by homoepitaxy of Sb_2S_3 at 160 °C (Figure 5).

conformal and perfectly uniaxial. As a bonus, judicious exploitation of surface energy effects can deliver unusual geometries, such as the rectangular wires converted from their cylindrical parents. Thus, the deposition of only two compounds, Sb_2S_3 and Sb_2Se_3, under various conditions using different combinations of two distinct growth modes enables one to create a wide variety of structures, including wires, tubes, core−shell wires, segmented wires, and rectangular wires (Figure 6). In all heteroepitaxial cases, the interface appears to be experimentally perfect, that is, it displays no crystal defects. No interdiffusion of the two materials is observed, in contrast to what has been shown to happen in many other cases.[15]

The core−shell structures presented here demonstrate the possibility of driving ALE at temperatures well below those used to date.[16] The growth of the double-segment structure relies on the high crystal anisotropy of a layered solid, which drives perfectly anisotropic growth in a manner reminiscent of the solvothermal growth of wires and rods.[17] The catalytic droplet is thus used to define the nanowire diameter initially, and then the face of highest surface energy is exposed for the growth of a second segment. We expect that this method will be adapted to other material systems featuring highly anisotropic crystal structures.

Acknowledgment. We thank M. Alexe and D. Hesse for helpful discussions and insightful comments. R.B.Y. was funded by the International Max Planck Research School for Science and Technology of Nanostructures with a predoctoral fellowship. This work was supported by the German Ministry of Education and Research (BMBF 03X5519) and the German Priority Program SPP 1386 on Nanostructured Thermoelectrics.

Supporting Information Available: Additional figures mentioned in the text (Figures S1−S3), larger versions of the HRTEM images presented in Figures 2−4 (Figures S4−S6), and experimental and theoretical methods. This material is available free of charge via the Internet at http://pubs.acs.org.

References

(1) George, S. M. *Chem. Rev.* **2010**, *110*, 111.
(2) Law, M.; Goldberger, J.; Yang, P. *Annu. Rev. Mater. Res.* **2004**, *34*, 83.
(3) (a) Wen, C.; Reuter, M. C.; Bruley, J.; Tersoff, J.; Kodambaka, S.; Stach, E. A.; Ross, F. M. *Science* **2009**, *326*, 1247. (b) Kim, C.; Lee, D.; Lee, H.; Lee, G.; Kim, G.; Jo, M. *Appl. Phys. Lett.* **2009**, *94*, 173105. (c) Zakharov, N.; Werner, P.; Gerth, G.; Schubert, L.; Sokolov, L.; Gošele, U. *J. Cryst. Growth* **2006**, *290*, 6. (d) Bjork, M. T.; Ohlsson, B. J.; Sass, T.; Persson, A. I.; Thelander, C.; Magnusson, M. H.; Deppert, K.; Wallenberg, L. R.; Samuelson, L. *Nano Lett.* **2002**, *2*, 87. (e) Wu, Y.; Fan, R.; Yang, P. *Nano Lett.* **2002**, *2*, 83. (f) Gudiksen, M. S.; Lauhon, L. J.; Wang, J.; Smith, D. C.; Lieber, C. M. *Nature* **2002**, *415*, 617. (g) Xiang, J.; Lu, W.; Hu, Y.; Wu, Y.; Yan, H.; Lieber, C. M. *Nature* **2006**, *441*, 489. (h) Hayden, O.; Greytak, A.; Bell, D. *Adv. Mater.* **2005**, *17*, 701. (i) Cui, L.; Ruffo, R.; Chan, C. K.; Peng, H.; Cui, Y. *Nano Lett.* **2009**, *9*, 491. (j) Lauhon, L. J.; Gudiksen, M. S.; Wang, D.; Lieber, C. M. *Nature* **2002**, *420*, 57. (k) Wang, K.; Chen, J.; Zhou, W.; Zhang, Y.; Yan, Y.; Pern, J.; Mascarenhas, A. *Adv. Mater.* **2008**, *20*, 3248.
(4) (a) Mohseni, P. K.; Maunders, C.; Botton, G. A.; LaPierre, R. R. *Nanotechnology* **2007**, *18*, 445304. (b) Zhou, H. L.; Hoang, T. B.; Dheeraj, D. L.; Helvoort, A. T. J. V.; Liu, L.; Harmand, J. C.; Fimland, B. O.; Weman, H. *Nanotechnology* **2009**, *20*, 415701.
(5) (a) Ahonen, M.; Pessa, M.; Suntola, T. *Thin Solid Films* **1980**, *65*, 301. (b) Koukitu, A.; Miyazawa, T.; Ikeda, H.; Seki, H. *J. Cryst. Growth* **1992**, *123*, 95. (c) Yao, T.; Takeda, T. *Appl. Phys. Lett.* **1992**, *48*, 160. (d) Wu, Y.; Toyoda, T.; Kawakami, Y.; Fujita, S.; Fujita, S. *Jpn. J. Appl. Phys.* **1990**, *29*, L727. (e) Dosho, S.; Takemura, Y.; Konagai, M.; Takahashi, K. *J. Appl. Phys.* **1989**, *66*, 2597.
(6) Melting points: Sb_2S_3, 550 °C; Sb_2Se_3, 611 °C.
(7) (a) Yang, R. B.; Bachmann, J.; Pippel, E.; Berger, A.; Woltersdorf, J.; Gošele, U.; Nielsch, K. *Adv. Mater.* **2009**, *21*, 3170. (b) Yang, R. B.; Bachmann, J.; Reiche, M.; Gerlach, J. W.; Gošele, U.; Nielsch, K. *Chem. Mater.* **2009**, *21*, 2586.
(8) (a) Zhang, Y.; Li, G.; Zhang, B.; Zhang, L. *Mater. Lett.* **2004**, *58*, 2279. (b) Lu, J.; Han, Q.; Yang, X.; Lu, L.; Wang, X. *Mater. Lett.* **2008**, *62*, 2415. (c) Wang, J.; Deng, Z.; Li, Y. *Mater. Res. Bull.* **2002**, *37*, 495. (d) Mernagh, T. P.; Trudu, A. G. *Chem. Geol.* **1993**, *103*, 113.
(9) Computed surface energies of the *a*, *b*, and *c* faces: 0.239, 0.254, and 0.311 J m^{-2}, respectively, for Sb_2S_3; 0.186, 0.226, and 0.293 J m^{-2}, respectively, for Sb_2Se_3.
(10) (a) Givargizov, E. *J. Cryst. Growth* **1975**, *31*, 20. (b) Wang, Y.; Chen, J.; Wang, P.; Chen, L.; Chen, Y.; Wu, L. *J. Phys. Chem. C* **2009**, *113*, 16009.
(11) Verheijen, M. A.; Immink, G.; de Smet, T.; Borgström, M. T.; Bakkers, E. P. A. M. *J. Am. Chem. Soc.* **2006**, *128*, 1353.
(12) (a) Shchetinin, A. A.; Nebol'sin, V. A.; Kozenkov, O. D.; Tatarenkov, A. F.; Dunaev, A. I.; Novokreshchenova, E. P. *Inorg. Mater.* **1991**, *27*, 1137. (b) Allen, J. E.; Hemesath, E. R.; Perea, D. E.; Lensch-Falk, J. L.; Li, Z. Y.; Yin, F.; Gass, M. H.; Wang, P.; Bleloch, A. L.; Palmer, R. E.; Lauhon, L. J. *Nat. Nanotechnol.* **2008**, *3*, 168. (c) Perea, D. E.; Allen, J. E.; May, S. J.; Wessels, B. W.; Seidman, D. N.; Lauhon, L. J. *Nano Lett.* **2006**, *6*, 181. (d) Kodambaka, S.; Tersoff, J.; Reuter, M. C.; Ross, F. M. *Phys. Rev. Lett.* **2006**, *96*, 096105. (e) Kodambaka, S.; Hannon, J. B.; Tromp, R. M.; Ross, F. M. *Nano Lett.* **2006**, *6*, 1292. (f) Hannon, J. B.; Kodambaka, S.; Ross, F. M.; Tromp, R. M. *Nature* **2006**, *440*, 69.
(13) Li, N.; Tan, T. Y.; Gošele, U. *Appl. Phys. A: Mater. Sci. Process.* **2008**, *90*, 591.
(14) (a) Paladugu, M.; Zou, J.; Guo, Y.-N.; Zhang, X.; Joyce, H. J.; Gao, Q.; Tan, H. H.; Jagadish, C.; Kim, Y. *J. Appl. Phys.* **2009**, *105*, 073503. (b) Paladugu, M.; Zou, J.; Guo, Y. N.; Auchterlonie, G. J.; Joyce, H. J.; Gao, Q.; Tan, H. H.; Jagadish, C.; Kim, Y. *Small* **2007**, *3*, 1873.
(15) González, J. C.; Malachias, A.; Andrade, R.; de Sousa, J.; Moreira, M.; de Oliveira, A. G. *J. Nanosci. Nanotechnol.* **2009**, *9*, 4673.
(16) All of the "low-temperature" ALE reactions reported to date were performed at or above 300 °C except for those in the following three reports: (a) Ohta, S.; Kobayashi, S.; Kaneko, F.; Kashiro, K. *J. Cryst. Growth* **1990**, *106*, 166. (b) Fujiwara, H.; Gotoh, J.; Shirai, H.; Shimizu, I. *J. Appl. Phys.* **1993**, *74*, 5510. (c) Luo, Y.; Slater, D.; Han, M.; Moryl, J.; Osgood, J. *Appl. Phys. Lett.* **1997**, *71*, 3799.
(17) (a) Peng, X.; Manna, L.; Yang, W.; Wickham, J.; Scher, E.; Kadavanich, A.; Alivisatos, A. P. *Nature* **2000**, *404*, 59. (b) Xi, L.; Tan, W. X. W.; Boothroyd, C.; Lam, Y. M. *Chem. Mater.* **2008**, *20*, 5444. (c) Cao, M.; Hu, C.; Peng, G.; Qi, Y.; Wang, E. *J. Am. Chem. Soc.* **2003**, *125*, 4982. (d) Kim, B.; Koo, T.; Lee, J.; Kim, D. S.; Jung, Y. C.; Hwang, S. W.; Choi, B. L.; Lee, E. K.; Kim, J. M.; Whang, D. *Nano Lett.* **2009**, *9*, 864. (e) Paek, J. H.; Nishiwaki, T.; Yamaguchi, M.; Sawaki, N. *Phys. Status Solidi C* **2009**, *6*, 1436. (f) Li, S.; Zhang, X.; Yan, B.; Yu, T. *Nanotechnology* **2009**, *20*, 495604. (g) Zhang, Y.; Tang, Y.; Lee, K.; Ouyang, M. *Nano Lett.* **2009**, *9*, 437.

JA102590V